energies

MDPI

Article

Electrochemical Evaluation of Surface Modified Free-Standing CNT Electrode for Li–O_2 Battery Cathode

Ji Hyeon Lee [1,2], Hyun Wook Jung [2], In Soo Kim [3], Min Park [4,5,*] and Hyung-Seok Kim [1,6,*]

1 Center for Energy Storage Research, Korea Institute of Science and Technology (KIST), Hwarang-ro 14-gil 5, Seongbuk-gu, Seoul 02792, Korea; 119514@kist.re.kr
2 Department of Chemical and Biological Engineering, Korea University, 145, Anam-ro, Seongbuk-gu, Seoul 02841, Korea; hwjung89@korea.ac.kr
3 Nanophotonics Research Center, Korea Institute of Science and Technology (KIST), Hwarang-ro 14-gil 5, Seongbuk-gu, Seoul 02792, Korea; isk@kist.re.kr
4 Major in Materials Science and Engineering, Hallym University, Chuncheon 24252, Korea
5 Integrative Materials Research Institute, Hallym University, Chuncheon 24252, Korea
6 Division of Energy and Environment Technology, KIST School, Korea University of Science and Technology, Seoul 02792, Korea
* Correspondence: minpark@hallym.ac.kr (M.P.); hskim0227@kist.re.kr (H.-S.K.); Tel.: +82-33-248-2363 (M.P.); +82-2-958-5281 (H.-S.K.)

Abstract: In this study, carbon nanotubes (CNTs) were used as cathodes for lithium–oxygen (Li–O_2) batteries to confirm the effect of oxygen functional groups present on the CNT surface on Li–O_2 battery performance. A coating technology using atomic layer deposition was introduced to remove the oxygen functional groups present on the CNT surface, and ZnO without catalytic properties was adopted as a coating material to exclude the effect of catalytic reaction. An acid treatment process (H_2SO_4:HNO_3 = 3:1) was conducted to increase the oxygen functional groups of the existing CNTs. Therefore, it was confirmed that ZnO@CNT with reduced oxygen functional groups lowered the charging overpotential by approximately 230 mV and increased the yield of Li_2O_2, a discharge product, by approximately 13%. Hence, we can conclude that the ZnO@CNT is suitable as a cathode material for Li–O_2 batteries.

Keywords: Li–O_2 battery; air cathode; CNT; oxygen functional groups; titration

Citation: Lee, J.H.; Jung, H.W.; Kim, I.S.; Park, M.; Kim, H.-S. Electrochemical Evaluation of Surface Modified Free-Standing CNT Electrode for Li–O_2 Battery Cathode. *Energies* **2021**, *14*, 4196. https://doi.org/10.3390/en14144196

Academic Editors: Hee-Dae Lim and Peter Foot

Received: 2 June 2021
Accepted: 7 July 2021
Published: 12 July 2021

1. Introduction

High-energy-density secondary batteries are required to address the increasing industrial needs for long-range electrical vehicles and large-scale energy storage systems and to support renewable energy sources. Commercialized secondary lithium-ion battery (LIB) technology does not reach sufficient energy density for the above future battery applications [1]. Under these circumstances, the lithium–oxygen (Li–O_2) battery, which has the highest theoretical capacity (3840 mAh g^{-1}) and energy density (~3500 Wh kg^{-1}), is attracting attention as a next-generation battery system to replace the current LIB [2–6]. Li–O_2 batteries operate by oxygen reduction reaction (ORR, $2Li^+ + O_2 + 2e^- \rightarrow Li_2O_2$) and oxygen evolution reaction (OER, $Li_2O_2 \rightarrow 2Li^+ + O_2 + 2e^-$), which are the Li_2O_2 processes of generation and decomposition [7]. Li–O_2 oxygen batteries use oxygen in the air, which is practically unlimited, free of cost, and environmentally friendly.

Several important technical challenges must be solved to commercialize Li–O_2 batteries [8–10]. First, the currently used carbonate-based organic electrolyte solvents, such as propylene carbonate, ethylene carbonate, and dimethyl carbonate, generate oxygen radicals (O_2^-) during the discharge reaction, and their high reactivity reacts with the electrolyte, resulting in electrolyte degradation [7,11,12]. The resultant electrolyte consumption is the major cause of the irreversibility of Li–O_2 batteries. Second, there is a safety issue due to the use of highly reactive lithium metal as an anode. Lithium metal is highly reactive with

oxygen and moisture, and when the charge and discharge reactions proceed, dendrites grow. This leads to the formation of an unstable interface and an eventual internal short circuit [13]. Many studies have been conducted to solve the above-mentioned problems; however, further improvement is required.

Another important issue with Li–O_2 batteries is the control of lithium peroxide (Li_2O_2) formation during the discharge reaction. Li_2O_2 is produced during discharge on the surface of the air electrode; therefore, an increase in capacity depends on the degree of air electrode porosity (Equation (1)):

$$2Li^+ + O_2 + 2e^- \rightarrow Li_2O_2 \quad (1)$$

Li_2O_2 is produced by reacting Li^+, air, and electrons diffused through the electrolyte during discharge. Two types of Li_2O_2 can be formed according to the generating pathway. The reduced oxygen and lithium ions of the electrolyte produce LiO_2, and the process of two LiO_2 molecules meeting to form Li_2O_2 is called a solution-mediated process. This process is as follows: $Li^+ + O_2^- \rightarrow LiO_2$, $2LiO_2 \rightarrow 2Li_2O_2 + O_2$. In this process, the formed Li_2O_2 has a toroidal shape, which has high capacity but is difficult to decompose. The other reaction is the surface film formation reaction in which LiO_2 and lithium ions combine to produce Li_2O_2. This process is as follows: $LiO_2 + Li^+ + e^- \rightarrow Li_2O_2$. It produces film-like Li_2O_2, which has lower capacity but is easier to decompose [3,14,15]. The ORR reaction does not tend toward only one process; both forms of products coexist. In this sense, air electrodes with pore structure that provides nucleation sites where optimally shaped Li_2O_2 can be formed will have high and reversible capacity.

For this reason, many carbon-based materials with mesopores (with pore size of 2–50 nm) and large specific surface area have been studied as potential air electrode materials for Li–O_2 batteries [16,17]. Carbon-based air electrodes produce byproducts (mainly Li_2CO_3) through H-abstraction reactions [8,18,19]; however, Li_2CO_3 is degraded at a higher voltage than the discharge product, Li_2O_2, during charging, which results in electrolyte decomposition. In addition, electrode clogging coming from the byproducts in carbon-based electrodes are one of the major issues for the performance of Li–O_2 batteries during ORR and OER reactions. When a discharge product (Li_2O_2) is formed in the ORR process, a byproduct is formed on the surface of the carbon-based electrode with the following reaction Equation: $Li_2O_2 + C + 1/2O_2 \rightarrow Li_2CO_3$. In the OER process, when Li_2O_2 meets an electrolyte and receives electrons, a byproduct in the form of $LiRCO_3$ is formed with following reaction Equation: $Li_2O_2 + e^-$ + electrolyte $\rightarrow LiRCO_3$ [20]. This reduces the reversibility of the cell and lowers the overall battery performance. Non-carbon material studies have also been conducted to solve this problem [21,22]. Non-carbon materials such as noble metals originally prevented side reaction production, but practical application has been hindered since they are heavy, expensive, and normally have far smaller surface area than carbon. According to Peng et al., nano porous gold (NPG) was used as an electrode instead of a carbon electrode to lower the charging overpotential and improve cyclability and rate capability [22]. These non-carbon-based studies continued and Luo et al. used a freestanding and stable 3D metal structure electrode for a lithium–air battery [21]. Despite these non-carbon-based studies, there is a limit to keeping up with the light and large specific surface area of carbon-based materials. Xia et al. studied the effect of different surface functional groups by controlling the concentration of NaClO solution [23]. In addition, Lee et al. controlled the action on the carbon surface through the heat treatment process for each temperature and studied the effect [24].

In this study, we attempted to determine the effect of surface functional groups on Li_2O_2 and the formation of other byproducts by controlling the concentration of oxygen functional groups on the carbon electrode. The more oxygen functional groups, the faster the $O^-{}_2$ reacts, resulting in a reaction that produces byproducts such as Li_2CO_3 and a surface-derived reaction that results in a film-like Li_2O_2 with a smaller capacity than the toroidal Li_2O_2.

Controlling side reactions through surface oxygen functional group control suppresses byproducts in ORR reactions and reduces charge overpotential in OER reactions. We

also modified the surface functional groups to lower the charge overpotential to close to 2.96 V, which is the generation/decomposition voltage of Li_2O_2. As carbon electrode material, we chose multi-walled carbon nanotubes (MWCNTs), which have large specific surface area (100–700 m^2 g^{-1}) and good electrical conductivity. First, we tried to examine the issues of the carbon electrode and tried to improve the surface of the MWCNTs by controlling the oxygen functional groups. Wet chemical etching was conducted to obtain a carbon electrode that maximized the oxygen functional groups (t-CNTs), and we confirmed that oxygen functional groups attached to MWCNTs are composed of hydroxyl (C–OH), carboxyl (COOH), and carbonyl (C=O) groups using X-ray photoelectron spectroscopy (XPS) analysis. We also obtained carbon electrodes with fewer oxygen functional groups through atomic layer deposition (ALD) treatment of the CNTs. ALD processing produced ZnO on the surface of MWCNTs where oxygen functional groups exist; this was intended to investigate the effect of oxygen functional groups on electrochemical properties [25].

2. Materials and Methods

2.1. Preparation of CNT Electrode with Controlled Oxygen Functional Groups

Free-standing electrodes were constructed using multi-layer wall CNTs (MWCNT-MR99) that were ball milled for 24 h. To prepare t-CNTs that contain many oxygen functional groups on the surface, ball-milled CNTs were sonicated in a strong acid solution (H_2SO_4:HNO_3 = 3:1) at 60 °C for 15 min [23]. Then, 0.14 g of prepared CNT was added (DI water:Isopropyl Alcohol = 4:1) and ultrasonicated for 20 min so that the mixture was distributed evenly. The above carbon mixture was then filtered under reduced pressure with sufficient DI water. Once the mixture was evenly dispersed in the filter, it was dried in an 80 °C oven for 10 min to obtain a CNT electrode that can be freestanding without any binder [26,27]. The freestanding CNT electrode has a nanowire shape, so it does not require a gas diffusion layer for the smooth dispersion of oxygen. To create a CNT with fewer oxygen functional groups, ZnO was coated on the t-CNT freestanding electrode using ALD (Veeco Savannah S200). The diethylzinc (DEZ) precursor was set to a 0.015 s pulse with H_2O. The exposure time was 3 s. The oxygen functional groups on the CNT surface react with the DEZ precursor. The ethyl group of DEZ reacts with the oxygen functional group to form ethane, and the remaining O and Zn form ZnO.

2.2. Characterization of CNTs with Controlled Oxygen Functional Groups

The nanowire morphology was confirmed by transmission electron microscopy (TEM, FEI Tecnai F20 G2), and elemental mapping images were obtained by scanning transmission electron microscopy energy dispersive X-ray spectroscopy (STEM-EDS) elemental mapping analysis XPS (PHI 5000 Versa Probe/ULCAC-PHI, Japan) using monochromatic Al K_α radiation ($h\nu$ = 1486.6 eV) was used to investigate the material properties of CNTs with oxygen functional groups controlled. Raman spectrometry was performed to identify the I_D/I_G ratio, which shows the determination of graphite crystallinity.

2.3. Electrochemical Characterization

The cathode for the Li–O_2 cell was composed of freestanding oxygen-functional-group-controlled CNT without any binder or additional gas diffusion layer for the even dispersion of air. The electrodes were ~2 mg cm^{-2}. A solution of 1 M lithium bis(trifluoromethane) sulfonamide (LiTFSI) in tetraethylene glycol dimethyl ether (TEGDME) was used as the electrolyte. The electrolyte contained less than 10 ppm H_2O so that it was not affected by water. This was measured using Karl Fisher titration. The electrodes were prepared as follows: lithium metal foil and separator (Whatman GF/F microfiber paper) were assembled with R2032 coin-type cells (R2030 coin-type/Wellcos Corp., Gyeonggi, Korea) in an argon-filled glovebox in which both H_2O and O_2 were less than 0.1 ppm. A hole with half the coin cell's diameter at the top of the cell allowed O_2 to flow to the electrode. The completed coin cell was placed in an HS air cell (an HS flat cell combined with a Swagelok type, EK cell/Wellcos Corp., Korea) to perform the electrochemical test. All

cells were operated in a pure oxygen (99.9%) atmosphere (1 bar) using a galvanostat (WBCS300M1/WonATech, Seoul, Korea) at a current density of 0.2 mA cm^{-2}. Every cell had a resting time of 30 min before operating to stabilize. The galvanostatic test for Li_2O_2 titration was also evaluated with a current density of 0.1 mA cm^{-2}. Each test was performed within a voltage window of 2.0–4.5 V vs. Li/Li^+.

2.4. Iodometric Titration

Electrodes are extracted from discharged cells in an Ar-filled glove box and placed in a vial. After taking the sealed vial out of the glove box, and we added 2 mL of DI water using a syringe, and stirred for 30 s or more for sufficient reaction with H_2O and Li_2O_2 generated on the CNT electrode. A drop of phenolphthalein was added to the vial, which served as an end point indicator, and titration with 0.005 M HCl solution was performed. After titration of the base, 2 wt% of KI in H_2O, 1mL of 3.5 M H_2SO_4, and 50 uL of Mo-based catalyst solution were added to the existing solution. The peroxide solution turns yellow when reagent is added due to I_2 formation, and the I_2 is immediately titrated to a pale-yellow color with 0.01 N NaS_2O_3. Then 0.5 mL of 1% starch indicator was added to the solution, and the solution turned a dark color and titration continued until the solution was clear. From the amount of NaS_2O_3 used, the amount of Li_2O_2 produced was calculated in reverse [28].

3. Results

3.1. Material Characterization of Prepared CNT Materials

CNTs are carbon isoforms with columnar-shaped nanostructures divided into single-walled and multi-walled nanotubes, depending on the number of nanotube walls. MWCNTs were chosen as a comparison group because of their high specific surface area, which can provide many Li_2O_2 generating sites leading to high capacity. The pore size and pore structure of the air electrode are closely related to the achievable capacity and reversibility of Li–O_2 batteries [29]. This is because the pore surfaces provide nucleation sites for discharge products [4]. As shown in Figure 1, we designed an experiment to investigate the effect of surface functional groups on the electrochemical properties of Li–O_2 batteries. This scheme also included methods for controlling oxygen functional groups. We expected that more oxygen functional groups on the surface of MWCNTs would result in the decreased integrity of the graphitic structure, reduced electrical conductivity, and electrolyte decomposition during charge and discharge, which would eventually increase the overpotential [29,30]. In order to prepare MWCNTs containing many oxygen functional groups, ball-milled MWCNTs were sonicated in a strong acid mixture (H_2SO_4:HNO_3 = 3:1) at 60 °C for 15 min—this sample was called treated CNT (t-CNT) [23]. For comparison, we also prepared MWCNTs with fewer oxygen functional groups by forming a transition metal oxide at the oxygen functional group using ALD (ZnO@CNT). We used diethylzinc (DEZ) for surface ALD processing to form ZnO, and in this system, we can exclude potential catalytic effects from the transition metal oxide [31–33]. During the ALD process, DEZ reacted with oxygen functional groups existing on the surface of CNT electrodes and the concentration of oxygen functional groups on the MWCNT surfaces could be modified.

For the air electrode, we prepared a current collector-free freestanding film using a one-step filtering process with pristine MWCNT, t-CNT, and ZnO@CNT. Figure 2a–d shows TEM images of the freestanding air electrode prepared from CNTs and EDS mapping images corresponding to C-, O-, and Zn-elements. Figures 2e–h and 2i–l show the TEM and EDS mapping images of t-CNT and ZnO@CNT in the same order, respectively. As can be seen in the TEM images (Figure 2a,e,i), we observed that acid treatment and ALD treatment did not affect the nanowire carbon structure. Figure 2c,g,k is an EDS mapping image of the O-element of the prepared electrode, showing that the oxygen functional groups are evenly distributed in the CNT, t-CNT, and ZnO@CNT. In addition, the mapping image of the c-element (Figure 2b,f,j) and the mapping image of the o-element (Figure 2c,g,k) show that t-CNT and ZnO@CNT have only changed the intensities of oxygen functional

groups. The intensity of the O-element of t-CNT electrodes compared with that of CNT or ZnO@CNT was higher, and when examining the atomic ratio of O in EDS analysis, the calculated values were 1.92% for the CNT electrode, 5.04% for the t-CNT electrode, and 1.62% for the ZnO@CNT electrode. As expected, the ZnO@CNT electrode, which was treated with ZnO using ALD, showed the fewest oxygen functional groups. Comparing Figure 2d,h,l, it can be seen that Zn is evenly distributed only in ALD-treated ZnO@CNT. As shown in Figure 2l, the EDS mapping image of the Zn-element has a stronger intensity around the surface. This means that in ALD treatment, DEZ reacts with oxygen functional groups present on the CNT electrode surface and can modify the oxygen functional group concentration on the MWCNT surface.

$$\vdash(OH)+Zn(C_2H_6)_2(g)\rightarrow\vdash O\text{-}Zn(C_2H_5)+C_2H_6(g) \quad (2)$$

$$\vdash O\text{-}Zn(C_2H_5)+H_2O\rightarrow\vdash O\text{-}Zn\text{-}(OH)+C_2H_6(g) \quad (3)$$

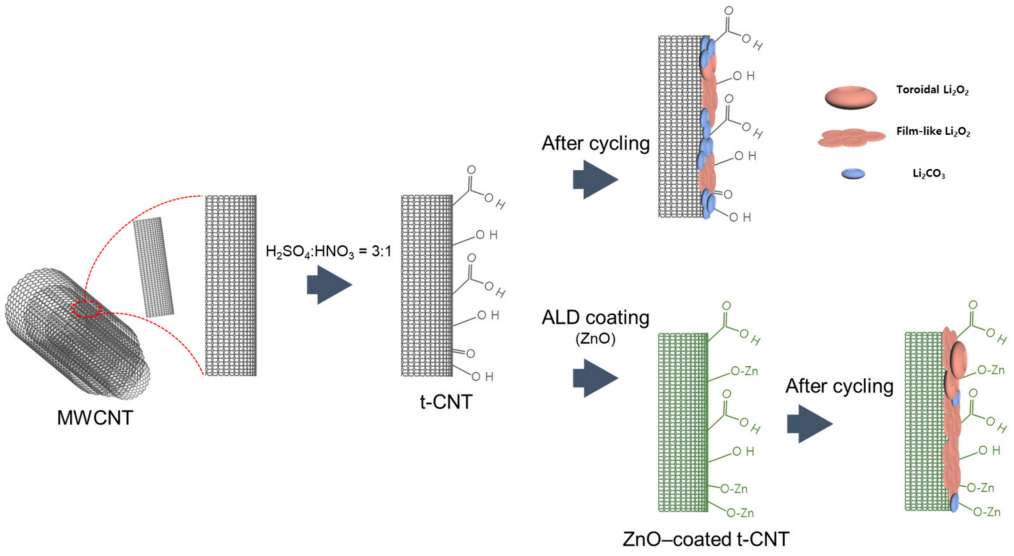

Figure 1. Scheme for the CNT functional groups modulation method.

Equation (2) is a reaction equation that occurs when DEZ meets the oxygen functional group on the CNT surface. One of the two ethyl groups of DEZ reacts with the surface oxygen functional group, and the remaining ethyl group reacts with H2O in Equation (3) and is blown away as ethane. Through this reaction equation, the ALD cycle is repeated to reduce oxygen functional groups. In the TEM EDS mapping image for each element, it was visually confirmed that the oxygen functional groups on the surface of the MWCNT were replaced by ZnO in ZnO@CNT due to the ALD treatment, and the oxygen functional groups were reduced. Although we could confirm via EDS analysis that the ZnO@CNT O-element intensity decreased, we attempted to further verify that the actual oxygen functional groups were controlled by surface treatments using XPS and Raman analysis.

XPS analysis was used to investigate the amount of oxygen functional group material and ZnO coating on the carbon surface; Figure 3 shows the XPS O 1 s spectra of the CNT, t-CNT, and ZnO@CNT electrodes. XPS spectra are separated by peaks at ~533.76, ~532.56, ~531.58, and 531.30 eV, corresponding to the binding energies of hydroxyl (C-OH), carboxyl (COOH), carbonyl (C=O), and the metal oxide (M-O) group, respectively [34–36]. The O=C peak that was not identified in the O 1 s spectra of the CNT electrode was observed in the O 1 s spectra of the t-CNT electrode. We calculated the O=C Gaussian area in the O 1 s spectra of t-CNTs, which was 22.58%. This clearly indicates that the oxygen functional groups were created after the wet etching process in t-CNTs (Figure 3a,b). In Figure 3c, we also calculated the O=C-O and C-O(H) Gaussian areas in the O 1 s spectra of the ZnO@CNT electrode, and the values decreased by 16% and 40.48%, respectively, compared with that

of the CNT electrode. From this result, we could confirm that the oxygen functional groups in the ZnO@CNT electrode were considerably decreased. The XPS spectrum shown in Figure 3c also shows that ALD treatment over bare MWCNTs reduced the amount of carbon defects because of the reduction of carboxyl peaks and the appearance of metal peaks [37]. In addition, the M-O peak in the O 1s spectra of the ZnO@CNT electrode indicated the formation of ZnO after ALD treatment. This result is consistent with the EDS analysis shown in Figure 2l.

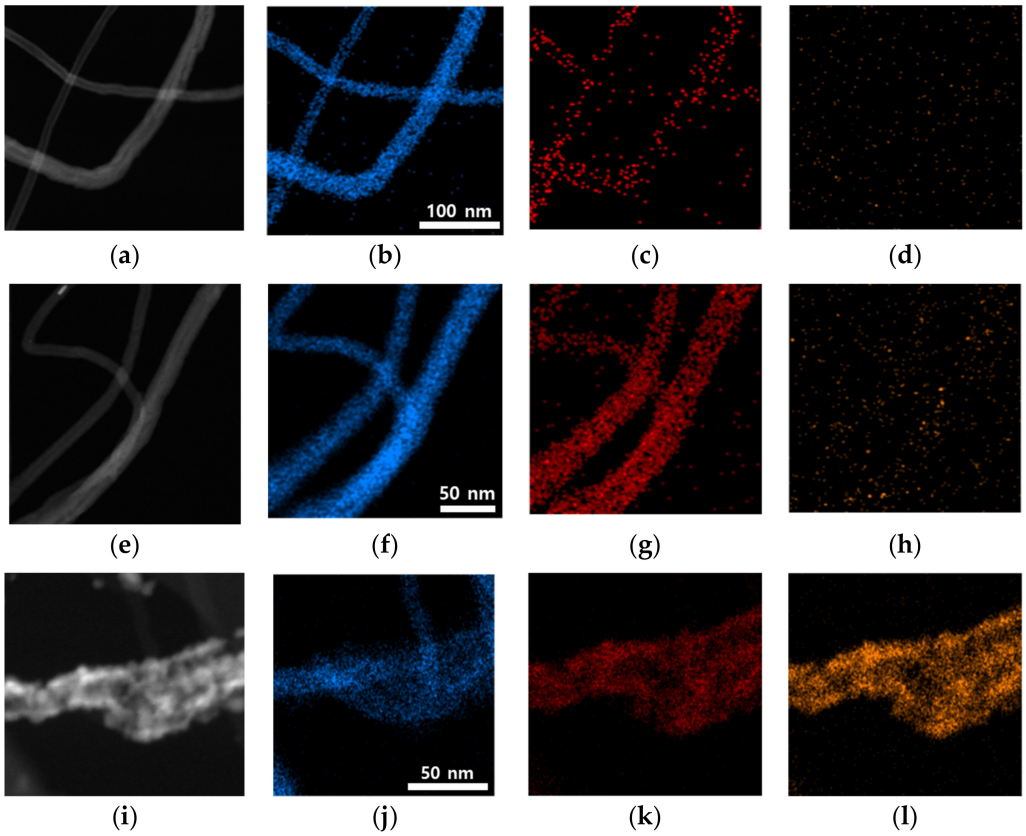

Figure 2. TEM images of each sample with controlled functional groups: (**a**) CNT; (**e**) t-CNT; (**i**) ZnO@CNT. Elemental mapping images for the carbon element of each sample: (**b**) CNT; (**f**) t-CNT; (**j**) ZnO@CNT. Elemental mapping images for the oxygen element of each sample: (**c**) CNT; (**g**) t-CNT; (**k**) ZnO@CNT. Elemental mapping images for the Zinc element of each sample: (**d**) CNT; (**h**) t-CNT; (**l**) ZnO@CNT.

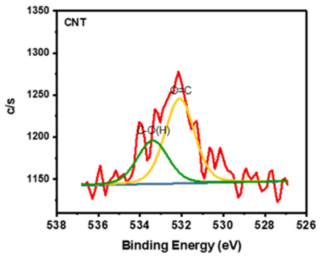

	Band (eV)	Gauss area (%)
C-O(H)	533.39	35.08
O=C-O	532.10	64.92

(**a**)

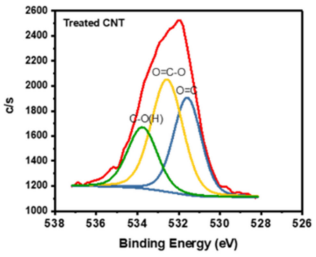

	Band (eV)	Gauss area (%)
C-O(H)	533.76	33.50
O=C-O	532.56	43.92
O=C	531.58	22.58

(**b**)

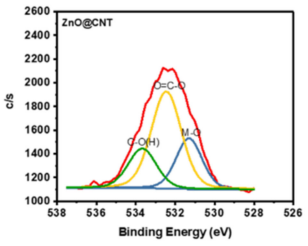

	Band (eV)	Gauss area (%)
C-O(H)	533.68	20.88
O=C-O	532.46	54.53
M-O	531.30	24.59

(**c**)

Figure 3. The XPS O 1 s spectra: (**a**) CNT; (**b**) t-CNT; (**c**) ZnO@CNT.

Figure 4 shows the Raman spectra of the CNT, t-CNT, and ZnO@CNT electrodes. We observed the D and G bands at wavenumbers of ~1350 and ~1580 cm^{-1}, respectively, for all electrodes; the D band is related to the amorphous, non-crystalline carbon (sp^3), and the G band is related to the graphite carbon (sp^2) [38]. The intensity ratio of the D and G bands (I_D/I_G) is generally used to evaluate the degree of defects in the graphite material. Thus, an increase in I_D/I_G suggests decreased graphite integrity; many defects exist, and this is normally observed in carbon materials containing many functional groups [30,39]. Therefore, we measured the I_D/I_G intensity ratio of the three freestanding electrodes and compared them. The values were 1.1, 0.95, and 0.92, for the t-CNT, CNT, and ZnO@CNT electrodes, respectively [40,41]. This result demonstrates that the I_D/I_G intensity ratio is correlated with the number of oxygen functional groups. This shows that there is a difference in the number of oxygen functional groups between the three electrodes, and the number of oxygen functional groups decreased in the order of t-CNTs, CNTs, and ZnO@CNTs. As the number of oxygen functional groups increases, graphite crystallinity decreases, accelerating electrolyte decomposition and leading to byproducts such as Li_2CO_3 [28].

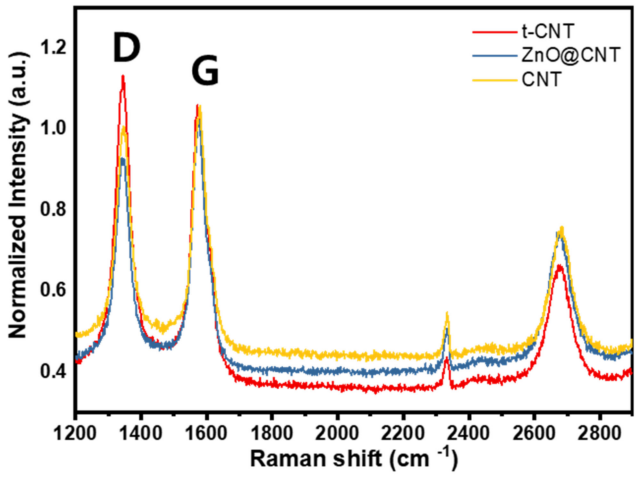

Figure 4. Raman data of comparison between t-CNT, ZnO@CNT, and CNT.

3.2. Electrochemical Properties of Prepared CNT Electrodes

To investigate the effect of oxygen functional groups on the electrochemical properties of carbon-based air electrodes, we prepared a coin-cell-type Li–O_2 battery cell and performed an electrochemical experiment. Figure 5 shows the charge/discharge voltage profiles of the CNT, t-CNT, and ZnO@CNT electrodes at a fixed capacity of 1000 mA h g^{-1}. In the first cycle, the observed overpotential of each electrode is shown in Figure 5a–c; the ZnO@CNT electrode had the lowest value of 0.99 V compared with 1.37 and 1.27 V for the CNT and t-CNT electrodes, respectively. We confirmed that the ZnO@CNT electrode contained the fewest oxygen functional groups among the three electrodes because the electrolyte decomposition occurring at the oxygen functional groups could be suppressed, and the generation of Li_2CO_3 byproduct is also reduced [35]. The increase in the number of oxygen functional groups on the CNT surface causes side reactions and electrolyte decomposition, which produces more byproducts such as Li_2CO_3 that lead to carbon electrode clogging [42]. In addition, the oxygen functional groups on the carbon surface lowered the carbon crystallinity and decreased the electrical conductivity, which caused a high overpotential of the electrode. We confirmed that the carbon electrodes containing fewer oxygen functional groups showed lower overpotential. This is identified in the same way as the intensity ratio of the previous I_D/I_G Raman data. In actual cell data, CNT or t-CNT electrodes with more oxygen functional groups than ZnO@CNT electrodes showed higher overpotential (Figure 5b,c). However, we observed higher overpotential with the CNT electrode than the t-CNT electrode; we found that the oxygen functional groups can help

the adsorption of oxygen, which can promote the oxygen reduction pathway to reduce the overpotential [17,29].

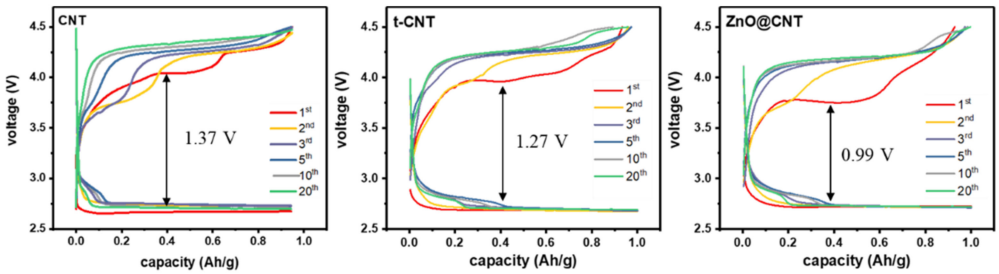

Figure 5. Discharge–charge voltage profiles at the fixed capacity of 1000 mA h g^{-1}: (**a**) CNT; (**b**) t-CNT; (**c**) ZnO@CNT.

3.3. The Yield Calculation for Li_2O_2 Formation by Iodine-Metric Titration

The iodine-metric titration method was used to determine the Li_2O_2 yield. This titration method can obtain the yield of the actual discharge product through a series of reaction equations, which can also measure the production of byproducts. The reaction equations are as follows:

$$Li_2O_2 + 2H_2O \rightarrow 2LiOH + H_2O_2 \quad (4)$$

$$H_2O_2 + 2KI + H_2SO_4 \rightarrow I_2 + K_2SO_4 + 2H_2O \quad (5)$$

$$I_2 + 2Na_2S_2O_3 \rightarrow Na_2S_4O_6 + 2NaI \quad (6)$$

By reacting each discharged air electrode with deionized water (DI water), lithium peroxide (Li_2O_2) generates hydrogen peroxide (H_2O_2) according to chemical reaction Equation (4). The acid and molybdic acid catalyst solution can react with iodine oxide to form iodine and then titrate with a thiosulfate solution to obtain Li_2O_2. This reaction follows Equations (5) and (6) [43,44]. The amount of Li_2O_2 produced during the first discharge of the two samples was compared (Table 1). To ensure the accuracy of the results, the average value of three experiments was used. The Li_2O_2 yields were calculated as 53.86%, 47.81%, and 43.80% for ZnO@CNTs, t-CNTs, and CNT, respectively. It was found that more discharge products formed in ZnO@CNTs than in other electrodes due to the effect of small number of oxygen functional groups on the surface. In the case of t-CNTs having more oxygen functional groups compared with CNTs, the ORR kinetics could be improved by promoting the oxygen reduction pathway, thereby resulting in a higher yield of Li_2O_2 compared with CNTs. The amount of Li_2O_2 is directly related to the observed capacity and the titration result explains high discharge capacity in ZnO@CNTs. The electrochemical test and titration results confirmed that the ZnO@CNT electrode having the fewest number of oxygen functional groups had the lowest overpotential and was more effective in forming Li_2O_2, leading to high capacity. These results prove that controlling the number of oxygen functional group on the surface of carbon electrodes for a Li–O_2 battery system greatly affects the yield of the discharge product and overpotential of the cell.

Table 1. Yield of Li_2O_2 after the first discharge as measured by iodine-metric titration.

0.1 mA cm^{-2}	ZnO@CNT	t-CNT	CNT
1	53.93%	45.56%	41.36%
2	53.26%	47.86%	45.67%
3	54.38%	49.88%	44.38%
Average	53.86%	47.81%	43.80%

4. Conclusions

In this work we tried to show that the control of CNT surface oxygen functional groups affect the amount of discharge product that determines discharge capacity and charging overpotential. To prove this, we increased oxygen functional groups on the CNT surface by simple acid treatment and reduced oxygen functional groups through ALD treatment. It is also worth noting that the prepared electrodes in this work were freestanding and did not require a binder or an extra gas diffusion layer. TEM, XPS, and Raman spectroscopy confirmed that the concentration of oxygen functional groups on the surface were controlled without structural change of CNT electrodes. Electrochemical test confirmed that the ZnO@CNT electrode with fewer oxygen functional groups than the CNT or t-CNT electrodes reduce the overpotential in the first charge. When the surface oxygen functional groups are reduced, side reactants such as $LiRCO_3$ due to electrolyte decomposition are suppressed. These byproducts cause surface clogging, which inactivates the electrode. On the other hand, if the surface oxygen functional group is increased, this reaction is accelerated, but it also promotes the oxygen reduction pathway to improve the ORR kinetics and lower the overpotential. The titration results also showed that byproduct formation due to electrolyte decomposition was reduced as the CNT oxygen functional groups decreased, which led to lower charging overpotential. In the ZnO@CNT electrode, the production of discharge products (Li_2O_2) increased, which indicate high discharge capacity. After electrochemical characterization and titration, it was confirmed that the proper control of oxygen functional groups affects the overpotential and the amount of discharge products. The effects after the first cycle are worth studying further. We are planning to investigate the effect of electrochemical cycles on the surface characteristics change for our next work and will try to find a way to maintain the first cycle effect for the successive cycles.

The results in this work suggest that controlling the number of oxygen functional groups is an important strategy for improving the electrochemical properties of carbon-based air electrodes for Li–O_2 batteries. From the electrochemical data, however, we observed that the reduced overpotential only maintained at the first cycle. This indicates that the electrode clogging issue due to byproducts is difficult to avoid in the carbon-based electrodes. We intend to discuss this in future studies, and it will also be interesting to study the degree of electrolyte decomposition depending on the type of oxygen functional groups.

Author Contributions: Conceptualization, I.S.K., M.P. and H.-S.K.; data curation, J.H.L.; writing—original draft preparation, J.H.L. and H.-S.K.; writing—review and editing, H.W.J. and M.P.; supervision, H.-S.K. All authors have read and agreed to the published version of the manuscript.

Funding: This research was funded by Hallym University Research Fund, 2021 (HRF- 202101-010).

Institutional Review Board Statement: Not applicable.

Informed Consent Statement: Not applicable.

Data Availability Statement: Not applicable.

Conflicts of Interest: The authors declare no conflict of interest.

References

1. Park, M.; Sun, H.; Lee, H.; Lee, J.; Cho, J. Lithium-air batteries: Survey on the current status and perspectives towards automotive applications from a battery industry standpoint. *Adv. Energy Mater.* **2012**, *2*, 780–800. [CrossRef]
2. Girishkumar, G.; McCloskey, B.; Luntz, A.C.; Swanson, S.; Wilcke, W. Lithium−air battery: Promise and challenges. *J. Phys. Chem. Lett.* **2010**, *1*, 2193–2203. [CrossRef]
3. Christensen, J.; Albertus, P.; Sanchez-Carrera, R.S.; Lohmann, T.; Kozinsky, B.; Liedtke, R.; Ahmed, J.; Kojic, A. A critical review of Li/air batteries. *J. Electrochem. Soc.* **2011**, *159*, R1. [CrossRef]
4. Lim, H.D.; Lee, B.; Bae, Y.; Park, H.; Ko, Y.; Kim, H.; Kim, J.; Kang, K. Reaction chemistry in rechargeable Li-O_2 batteries. *Chem. Soc. Rev.* **2017**, *46*, 2873–2888. [CrossRef] [PubMed]
5. Geng, D.; Ding, N.; Hor, T.A.; Chien, S.W.; Liu, Z.; Wuu, D.; Sun, X.; Zong, Y. From Lithium-Oxygen to Lithium-Air Batteries: Challenges and Opportunities. *Adv. Energy Mater.* **2016**, *6*, 1502164. [CrossRef]

6. Bruce, P.G.; Freunberger, S.A.; Hardwick, L.J.; Tarascon, J.-M. Li-O_2 and Li-S batteries with high energy storage. *Nat. Mater.* **2012**, *11*, 19. [CrossRef] [PubMed]
7. Bryantsev, V.S.; Uddin, J.; Giordani, V.; Walker, W.; Addison, D.; Chase, G.V. The identification of stable solvents for nonaqueous rechargeable Li-air batteries. *J. Electrochem. Soc.* **2012**, *160*, A160. [CrossRef]
8. Freunberger, S.A.; Chen, Y.; Peng, Z.; Griffin, J.M.; Hardwick, L.J.; Bardé, F.; Novák, P.; Bruce, P.G. Reactions in the rechargeable lithium-O_2 battery with alkyl carbonate electrolytes. *J. Am. Chem. Soc.* **2011**, *133*, 8040–8047. [CrossRef]
9. McCloskey, B.; Speidel, A.; Scheffler, R.; Miller, D.; Viswanathan, V.; Hummelshøj, J.; Nørskov, J.; Luntz, A. Twin problems of interfacial carbonate formation in nonaqueous Li-O_2 batteries. *J. Phys. Chem. Lett.* **2012**, *3*, 997–1001. [CrossRef] [PubMed]
10. Ogasawara, T.; Débart, A.; Holzapfel, M.; Novák, P.; Bruce, P.G. Rechargeable Li_2O_2 electrode for lithium batteries. *J. Am. Chem. Soc.* **2006**, *128*, 1390–1393. [CrossRef] [PubMed]
11. Read, J. Characterization of the lithium/oxygen organic electrolyte battery. *J. Electrochem. Soc.* **2002**, *149*, A1190. [CrossRef]
12. Abraham, K.; Jiang, Z. A polymer electrolyte-based rechargeable lithium/oxygen battery. *J. Electrochem. Soc.* **1996**, *143*, 1. [CrossRef]
13. Itkis, D.M.; Semenenko, D.A.; Kataev, E.Y.; Belova, A.I.; Neudachina, V.S.; Sirotina, A.P.; Hävecker, M.; Teschner, D.; Knop-Gericke, A.; Dudin, P. Reactivity of carbon in lithium–oxygen battery positive electrodes. *Nano Lett.* **2013**, *13*, 4697–4701. [CrossRef] [PubMed]
14. Aetukuri, N.B.; McCloskey, B.D.; García, J.M.; Krupp, L.E.; Viswanathan, V.; Luntz, A.C. Solvating additives drive solution-mediated electrochemistry and enhance toroid growth in non-aqueous Li-O_2 batteries. *Nat. Chem.* **2015**, *7*, 50–56. [CrossRef]
15. Oh, D.; Qi, J.; Lu, Y.-C.; Zhang, Y.; Shao-Horn, Y.; Belcher, A.M. Biologically enhanced cathode design for improved capacity and cycle life for lithium-oxygen batteries. *Nat. Commun.* **2013**, *4*, 2756. [CrossRef] [PubMed]
16. Li, Q.; Cao, R.; Cho, J.; Wu, G. Nanostructured carbon-based cathode catalysts for nonaqueous lithium–oxygen batteries. *Phys. Chem. Chem. Phys.* **2014**, *16*, 13568–13582. [CrossRef] [PubMed]
17. Ottakam Thotiyl, M.M.; Freunberger, S.A.; Peng, Z.; Bruce, P.G. The carbon electrode in nonaqueous Li-O_2 cells. *J. Am. Chem. Soc.* **2013**, *135*, 494–500. [CrossRef]
18. Andrieux, C.P.; Hapiot, P.; Saveant, J.M. Mechanism of superoxide ion disproportionation in aprotic solvents. *J. Am. Chem. Soc.* **1987**, *109*, 3768–3775. [CrossRef]
19. Frimer, A.A.; Farkash-Solomon, T.; Aljadeff, G. Mechanism of the superoxide anion radical (O2-) mediated oxidation of diarylmethanes. *J. Org. Chem.* **1986**, *51*, 2093–2098. [CrossRef]
20. McCloskey, B.D.; Bethune, D.; Shelby, R.; Mori, T.; Scheffler, R.; Speidel, A.; Sherwood, M.; Luntz, A. Limitations in rechargeability of Li-O_2 batteries and possible origins. *J. Phys. Chem. Lett.* **2012**, *3*, 3043–3047. [CrossRef]
21. Luo, N.; Ji, G.-J.; Wang, H.-F.; Li, F.; Liu, Q.-C.; Xu, J.-J. Process for a Free-Standing and Stable All-Metal Structure for Symmetrical Lithium–Oxygen Batteries. *ACS Nano* **2020**, *14*, 3281–3289. [CrossRef]
22. Peng, Z.; Freunberger, S.A.; Chen, Y.; Bruce, P.G. A reversible and higher-rate Li-O_2 battery. *Science* **2012**, *337*, 563–566. [CrossRef]
23. Xia, G.; Shen, S.; Zhu, F.; Xie, J.; Hu, Y.; Zhu, K.; Zhang, J. Effect of oxygen-containing functional groups of carbon materials on the performance of Li-O_2 batteries. *Electrochem. Commun.* **2015**, *60*, 26–29. [CrossRef]
24. Lee, M.; Yoo, Y.; Kwak, J.H.; Yun, Y.S.; Jung, H.-G.; Byun, D.; Oh, S.H.; Lim, H.-D. Effect of surface characteristics of carbon host on electrochemical performance of nonaqueous Li-O_2 batteries. *Chem. Eng. J.* **2021**, *412*, 128549. [CrossRef]
25. Débart, A.; Paterson, A.J.; Bao, J.; Bruce, P.G. α-MnO_2 nanowires: A catalyst for the O_2 electrode in rechargeable lithium batteries. *Angew. Chem. Int. Ed.* **2008**, *47*, 4521–4524. [CrossRef]
26. De Menezes, B.; Ferreira, F.; Silva, B.; Simonetti, E.; Bastos, T.; Cividanes, L.; Thim, G. Effects of octadecylamine functionalization of carbon nanotubes on dispersion, polarity, and mechanical properties of CNT/HDPE nanocomposites. *J. Mater. Sci.* **2018**, *53*, 14311–14327. [CrossRef]
27. Xiao, J.; Mei, D.; Li, X.; Xu, W.; Wang, D.; Graff, G.L.; Bennett, W.D.; Nie, Z.; Saraf, L.V.; Aksay, I.A. Hierarchically porous graphene as a lithium–air battery electrode. *Nano Lett.* **2011**, *11*, 5071–5078. [CrossRef]
28. McCloskey, B.D.; Valery, A.; Luntz, A.C.; Gowda, S.R.; Wallraff, G.M.; Garcia, J.M.; Mori, T.; Krupp, L.E. Combining accurate O_2 and Li_2O_2 assays to separate discharge and charge stability limitations in nonaqueous Li-O_2 batteries. *J. Phys. Chem. Lett.* **2013**, *4*, 2989–2993. [CrossRef]
29. Ferreira, F.; Francisco, W.; Cividanes, L.; Coutinho, A.; Thim, G. Dodecylamine Functionalization of Cnt: Thermal Stability And Dispersion. *Blucher Chem. Eng. Proc.* **2015**, *1*, 2421–2426.
30. Lu, Y.-C.; Gasteiger, H.A.; Shao-Horn, Y. Catalytic activity trends of oxygen reduction reaction for nonaqueous Li-air batteries. *J. Am. Chem. Soc.* **2011**, *133*, 19048–19051. [CrossRef]
31. Yang, C.; Wong, R.A.; Hong, M.; Yamanaka, K.; Ohta, T.; Byon, H.R. Unexpected Li_2O_2 film growth on carbon nanotube electrodes with CeO_2 nanoparticles in Li-O_2 batteries. *Nano Lett.* **2016**, *16*, 2969–2974. [CrossRef]
32. Biniak, S.; Szymański, G.; Siedlewski, J.; Świątkowski, A. The characterization of activated carbons with oxygen and nitrogen surface groups. *Carbon* **1997**, *35*, 1799–1810. [CrossRef]
33. Largani, S.H.; Pasha, M.A. The effect of concentration ratio and type of functional group on synthesis of CNT–ZnO hybrid nanomaterial by an in situ sol–gel process. *Int. Nano Lett.* **2017**, *7*, 25–33. [CrossRef]

34. Sadri, R.; Hosseini, M.; Kazi, S.; Bagheri, S.; Zubir, N.; Solangi, K.; Zaharinie, T.; Badarudin, A. A bio-based, facile approach for the preparation of covalently functionalized carbon nanotubes aqueous suspensions and their potential as heat transfer fluids. *J. Colloid Interface Sci.* **2017**, *504*, 115–123. [CrossRef]
35. Sadri, R.; Hosseini, M.; Kazi, S.; Bagheri, S.; Zubir, N.; Ahmadi, G.; Dahari, M.; Zaharinie, T. A novel, eco-friendly technique for covalent functionalization of graphene nanoplatelets and the potential of their nanofluids for heat transfer applications. *Chem. Phys. Lett.* **2017**, *675*, 92–97. [CrossRef]
36. Lu, J.; Lei, Y.; Lau, K.C.; Luo, X.; Du, P.; Wen, J.; Assary, R.S.; Das, U.; Miller, D.J.; Elam, J.W. A nanostructured cathode architecture for low charge overpotential in lithium-oxygen batteries. *Nat. Commun.* **2013**, *4*, 2383. [CrossRef] [PubMed]
37. Ferrari, A.C.; Meyer, J.; Scardaci, V.; Casiraghi, C.; Lazzeri, M.; Mauri, F.; Piscanec, S.; Jiang, D.; Novoselov, K.; Roth, S. Raman spectrum of graphene and graphene layers. *Phys. Rev. Lett.* **2006**, *97*, 187401. [CrossRef] [PubMed]
38. Das, A.; Pisana, S.; Chakraborty, B.; Piscanec, S.; Saha, S.K.; Waghmare, U.V.; Novoselov, K.S.; Krishnamurthy, H.R.; Geim, A.K.; Ferrari, A.C. Monitoring dopants by Raman scattering in an electrochemically top-gated graphene transistor. *Nat. Nanotechnol.* **2008**, *3*, 210–215. [CrossRef]
39. Deboever, J. *Characterization of Lithium Peroxide Formation in Lithium Air Battery Electrode Via Titration Techniques and EIS*; Oregon Institute of Technology: Klamath Falls, OR, USA, 2014.
40. Jia, H.; Li, X.; Song, J.; Zhang, X.; Luo, L.; He, Y.; Li, B.; Cai, Y.; Hu, S.; Xiao, X. Hierarchical porous silicon structures with extraordinary mechanical strength as high-performance lithium-ion battery anodes. *Nat. Commun.* **2020**, *11*, 1474. [CrossRef]
41. Kim, K.i.; Guo, Q.; Tang, L.; Zhu, L.; Pan, C.; Chang, C.h.; Razink, J.; Lerner, M.M.; Fang, C.; Ji, X. Reversible Insertion of Mg-Cl Superhalides in Graphite as a Cathode for Aqueous Dual-Ion Batteries. *Angew. Chem.* **2020**, *132*, 20096–20100. [CrossRef]
42. Lim, H.-D.; Park, K.-Y.; Gwon, H.; Hong, J.; Kim, H.; Kang, K. The potential for long-term operation of a lithium–oxygen battery using a non-carbonate-based electrolyte. *Chem. Commun.* **2012**, *48*, 8374–8376. [CrossRef]
43. Elizabeth, I.; Mathur, R.; Maheshwari, P.; Singh, B.; Gopukumar, S. Development of SnO_2/multiwalled carbon nanotube paper as free standing anode for lithium ion batteries (LIB). *Electrochim. Acta* **2015**, *176*, 735–742. [CrossRef]
44. Yue, L.; Zhong, H.; Zhang, L. Enhanced reversible lithium storage in a nano-Si/MWCNT free-standing paper electrode prepared by a simple filtration and post sintering process. *Electrochim. Acta* **2012**, *76*, 326–332. [CrossRef]